CHAPTER V
MORPHOLOGY STUDY OF MFI ZEOLITE SYNTHESIZED DIRECTLY FROM SILATRANE AND ALUMATRANE VIA THE SOL-GEL PROCESS AND MICROWAVE HEATING

5.1 Abstract

Silatrane and alumatrane were prepared via the oxide one-pot process, and used as precursors for synthesis of MFI. The effect on MFI morphology of tetrabutyl ammonium hydroxide (TBA) and tetrapropyl ammonium bromide (TPA) as organic templates was compared. The influence of aging time, and of the sodium and hydroxide content of alumatrane were also investigated. TPA shows better performance as a template for the MFI synthesis than TBA by decreasing aging and heating times. Different templates produce different morphologies and growth directions of MFI crystals due to the steric effect of the template molecule. Increase of alumatrane loading retards MFI crystal formation, but no significant effect is observed on varying sodium and hydroxide concentrations as previously found for pure silicate MFI.

5.2 Introduction

ZSM5 or MFI zeolite has become an increasingly important zeolite over the past decade as it has found a variety of applications, especially in the petrochemical industry. Here, the major uses are in reforming processes because it is a strong acid catalyst. One example is its application as an octane booster via the cracking of alkanes on H-ZSM5, known to be a selective catalyst which cracks only linear hydrocarbons and preseves branched alkanes. MFI has a uniformity of pore size that enhances specific interaction with selected hydrocarbons. Moreover, it is also used as a metal catalyst support due to its high thermal stability and high surface area.

MFI is a synthetic zeolite, not found in nature due to a formation of a unique pore structure requiring the presence of an organic molecule as a template or guest species to stabilize the pore. Relative to other types of zeolite, MFI is a high silicate type, containing only a few aluminum atoms or other heteroatoms substituted in the structure. In the case of high aluminum MFI, it is known that use of a template can be exempted [1], whereas the synthesis of pure silicate MFI cannot succeed without a template. Several templates from the family of tetraalkylammonium salts or hydroxides have been examined [2-7] in MFI synthesis, and their mode of action evaluated using theoretical calculation [8-9]. Recent work indicates that the tetrapropylammonium (TPA) salt is the template of choice for MFI synthesis [5,10-18].

Inorganic compounds such as fumed silica, silicic acid, and sodium silicate as well as organosilicates such as tetraethoxysilane, were studied as sources of silica for MFI synthesis by De Moor et al [5-6,13] and Martens et al [14-16]. These authors investigated the nucleation and growth mechanism of MFI formation in the presence of TPA as template. However, recently, it has been shown that by using a novel precursor, silatrane, MFI can be successfully synthesized using tetrabutylammonium hydroxide (TBA) [19]. Normally TBA prefers to form ZSM11 or MEL zeolite topology, as demonstrated by Kirschhock et al [16] using x-ray scattering analysis. Burchart et al [20] studied both templates and explained the preferential interactions between these templates with MEL and MFI by molecular mechanics calculation. Two properties, which make silatrane different from other organosilicates, are

decreased susceptibility to hydrolysis by water, and release of larger ligands during hydrolysis. As discussed later, these effects may act to yield MFI formation.

Both silatrane and alumatrane have been used successfully as precursors for synthesis of microporous [19,21-22] and mesoporous [23] zeolites via the sol-gel process. As a continuation of these studies, we investigate here the effect of the templates, TBA and TPA, on the synthesis of pure silicate and aluminosilicate MFI, including the influence of formulation variables and reaction conditions.

5.3 Experimental

Materials

Fumed silica with silica content 99.8% (SiO_2) was supplied from Sigma Chemical. Aluminum hydroxide hydrate ($Al(OH)_3.xH_2O$) was purchased from Aldrich Chemical Co. Inc. (USA). Triethanolamine (TEA, $N[CH_2CH_2OH]_3$) was supplied by Carlo Erba reagenti. Triisopropanolamine (TIS, $N[CH_2CHCH_3OH]_3$) was obtained from Fluka Chemika-BioChemika (Switzerland). Ethylene glycol (EG), used as reaction solvent, was obtained from J.T. Baker. Sodium hydroxide (NaOH) and sodium chloride (NaCl) were purchased from EKA Chemicals and AJAX chemicals, respectively. Tetra-butyl ammonium hydroxide (TBAOH) and tetra-propyl ammonium bromide (TPA) were obtained from Fluka Chemical AG. All chemicals were used as received. Acetonitrile (CH_3CN) was obtained from Lab-Scan Co., Ltd. and distilled using standard purification methods prior to use.

Instrumentation

FTIR spectroscopic analysis was conducted using a Bruker Instrument spectrometer (EQUINOX55) with a resolution of 2 cm^{-1} to measure the functional groups of materials. The solid samples were mixed and pelletized with dried KBr. Mass spectrometry was carried out using a VG Autospec model 7070E from Fison Instruments with VG data system, in the positive fast atomic bombardment (FAB^+-MS) mode and with glycerol as the matrix. CsI was used as a reference, and a cesium gun was used as an initiator. The mass range covered was from m/e = 20 to 3,000. Thermal properties and stability were analyzed using a Perkin Elmer TGA7 analyzer at a scanning rate of 10°C/min under nitrogen atmosphere, and simultaneous thermal analysis (STA) was conducted using Netzsch instrument STA 409 at a scanning rate of 20°C/min under nitrogen and oxygen atmosphere. The crystal morphology was studied using a JEOL 5200-2AE scanning electron microscope. Crystal structure was characterized using a Rigaku X-Ray Diffractometer at a scanning speed of 5 degree/sec, with Cu K line as incident radiation and a filter. The working range was 3-50 theta/2 theta, with 1 degree and 0.3 mm setting of divergence for the scattering

and receiving slits, respectively. The Si/Al ratio was measured by X-ray fluorescence spectroscopy (Bruker model SRS 3400), with 99.8% boric acid as binder. Hydrothermal treatment by microwave heating technique was conducted using MSP1000, CME cooperation (Spec 1,000 W and 2450 MHz). Samples were heated in a Teflon tube, using the inorganic digestion mode, with time-to-temperature programming.

Methodology

Alumatrane synthesis

Alumatrane (tris(alumatranyloxy-i-propyl)amine or AlTIS) was synthesized using the method reported by Wongkasemjit et al [24] by mixing 0.125 mole TIS and 0.1 mole $Al(OH)_3$ in 100 ml of EG. EG was removed after completion of the reaction by distillation under vacuum (8 mm Hg) at 110 °C until dry crude product was obtained. The pale-yellow solid was washed three times with dried acetonitrile to obtain a fine white powder. The purified product was characterized using XRD, TGA, FTIR and FAB^+-MS.

Silatrane synthesis

Silatrane (tris(silatranyloxy-ethyl)amine or SiTEA) was synthesized using methodology identical to that for alumatrane synthesis by heating a mixture of 0.125 mol TEA, 0.1 mol SiO_2 and 100 ml of EG at 200 °C under nitrogen atmosphere. The reaction was completed within 10 h and the mixture was cooled to room temperature before distilled off the excess EG under vacuum (8 mmHg) at 110 °C for 3 h. The brownish white solid was washed three times with dried acetonitrile to obtain a fine white powder. The silatrane product was characterized using XRD, TGA, FTIR and FAB^+-MS.

Synthesis of pure silicate MFI

SiTEA equivalent to 0.25 g SiO_2 was dispersed in 5 ml of water and continuously stirred before adding the template molecule (TBA or TPA). In the case of TBA template, NaOH was added to balance the total hydroxide, and NaCl was

added to balance the sodium ion concentration (Na^+). In the case of the TPA template, NaOH was added to reach desired hydroxide concentration, NaCl was used for adjusting total sodium ion concentration. Water was then added to all samples, according to the stoichiometric formula. To establish the optimum reaction conditions for pure silicate MFI synthesis with the two templates, TBA and TPA, as in previous work [19], the heating times at 150 °C was fixed and aging times at room temperature were systematically varied. The formulation was fixed at the mole ratio of SiO_2:template:OH^-:Na^+:H_2O = 1:0.1:0.4:0.4:114. Prior to heating, all prepared samples were aged for different periods of time at room temperature with continuous stirring.

Synthesis of Aluminosilicate MFI

Since alumatrane is more susceptible to hydrolysis by water, it was added at the end of the above-specified procedure to prepare pure silicate MFI. Again, ratios of Si/Al, OH^- and Na^+ concentration, and the time period for addition of alumatrane were varied to elucidate their influence on the morphology of aluminosilicate MFI crystals in both TPA and TBA template systems.

5.4 Results and Discussion

Silatrane and alumatrane were successfully synthesized via the Oxide One Pot Synthesis (OOPS) synthesis. The crude as-synthesized products, alumatrane and silatrane, obtained before distilling off the excess EG, were characterized using FAB^+-MS, as shown in tables 5.1 and 5.2, respectively. FTIR spectra confirm the presence of the characteristic peaks of the silatrane and alumatrane products, as follows. Silatrane: 3422 cm^{-1} (ν OH), 2986-2861 cm^{-1} (ν CH), 2697 cm^{-1} (ν N→Si), 1459-1445 cm^{-1} (δ CH), 1351 cm^{-1} (ν CN), 1082 cm^{-1} (ν Si-O-C), 1049 cm^{-1} (ν CO), 579 cm^{-1} (ν N→Si). Alumatrane: 3404 cm^{-1} (ν OH), 2937-2881 cm^{-1} (ν CH), 1650 cm^{-1} (ν OH overtone), 1460 cm^{-1} (δ CH), 1089 cm^{-1} (ν Al-O-C) and 500-800 cm^{-1} (ν Al-O).

XRD analysis was carried out to confirm that these two products have their characteristic crystal structures, as shown in figure 5.1, although the diffraction pattern of alumatrane (Figure 5.1(a)) indicates the presence of some amorphous starting material, $Al(OH)_3$. The char yields of both silatrane and alumatrane are shown in figure 5.2. Silatrane exhibits only one weight loss transition at around 400°C, corresponding to the decomposition of organic ligand. The char yield is around 20%, which is close to the theoretical yield of $Si((OCH_2CH_2)_3N)_2H_2$ (18.4 %). Alumatrane shows two major transitions at 140° and 380°C, corresponding to decomposition of EG solvent trapped in the product powder and the organic ligand, respectively. The final char yield, ~30%, is black in color and larger than the theoretical value, 23.72%, by 6%, presumably due to incomplete combustion.

MFI Synthesis

In this work, TPA and TBA were used as the templates for producing MFI. As noted earlier, while previous work [16,20] shows that TBA is a MEL directing agent our studies [19] show that TBA with silatrane as precursor produces MFI. Following our previous study [19], the formulation used is SiO_2: 0.1TBA(or 0.1TPA): $0.4OH^-$: $0.4Na^+$: $114H_2O$. With TBA, our previous study [19] showed that the optimal aging and heating times were 84 h at room temperature and 15 h at

150°C, respectively. With TPA, it was necessary to investigate the effect of variable aging times.

Effect of aging and heating time on pure Si-MFI using TPA and TBA templates

From our previous work [19], we know that either too high or too low Na^+ and OH^- concentration gives poor results for pure Si-MFI synthesis. Thus, we utilized the same formulation for TPA as for TBA, i.e. SiO_2: 0.1TPA: 0.4Na: 0.4OH: $114H_2O$. Since TPA is a more efficient template for MFI than TBA, we used a shorter heating time, 10 h. The SEM results from different aging times are shown in figure 5.3. Surprisingly, the MFI obtained using TPA shows a different crystal morphology compared to that observed in our earlier study with TBA as template [19]. As illustrated in Figure 5.4, the TBA template results in rectangular crystals elongated along the crystal c-axis (Figure 5.4a), whereas square crystals are formed, when using the TPA template (Figure 5.4b). Moreover, with the TBA template, the crystals tend to grow in size, and contain less amorphous material as the aging time increases [19]. In contrast, as seen in Figure 5.3, when using the TPA template, large crystals are formed at short aging times, together with some crystal scrap, probably due to cracking of crystals that are too large. Apparently, decrease of aging time results in less nucleation with TPA, as a result, producing larger crystals. However, both TPA and TBA show the same correlation that more perfect crystals are obtained with increasing aging time.

The distinct morphological features observed when comparing these two templates likely originate from steric hindrance during crystal formation. These dissimilarities arise because the length of alkyl chain of TBA is longer than that of TPA. Indeed, differences in the mechanism of nanoslab aggregation due to the different steric interaction associated with TPA and TBA templates has been suggested as the source of the preferential formation of MFI by TPA and MEL by TBA [16,20]. The sinusoidal open channels lie along the a-axis and the straight open channels lie along the b-axis, therefore the longer alkyl chains of TBA tend to encounter greater steric hindrance in growth along these directions. Thus, crystal formation with TBA tends to grow along the c-axis rather than along the a- or b-directions. Molecular mechanics modelling [20] indicates that the difference in

stability of MFI and MEL zeolite structures, using TPA versus TBA as templates, is marginal when the zeolite voids are not completely filled by template molecules. Thus we speculate that when using silatrane as a precursor, because of its decreased susceptibility to hydrolysis, the MFI structure may be kinetically favored.

Our previous XRD results in the case of TBA as template [19], when the heating time was varied, support this interpretation, as shown in figure 5.5a. After heating for 5 h, with samples aged for 84 h, two barely perceptible peaks (see arrows) are observed near 9 /2theta and 8 /2theta, which correspond to the expected positions of the 8.89 (020), 8.83 (200) and 7.95 (101) diffraction maxima. After 10 h heating, the peak near 9/2theta dramatically increases compared to the peak at 8/2theta, which shows a smaller increment. However, on further heating, the peak at 8/2theta continues to increase, whereas the peak at 9/2theta diminishes. This evidence supports that the crystals obtained using the TBA template have steric hindrance, which inhibits the crystal to grow along the a- and b-directions. By shortening the alkyl chain as in TPA, less steric hindrance occurs, enabling the crystals to grow more easily in the a- and b-directions. Thus, the shape of the crystals with TPA becomes square whereas those obtained using TBA are rectangular.

On varying the heating time between 5, 10 and 15 for 60 hour aged samples, no change in XRD patterns was observed (Figure 5.5b), when using TPA as template. More perfect crystals are formed at shorter heating times with TPA compared with TBA. From previous work [19] using the TBA template under equivalent conditions, i.e. 60 hr aging time, crystals with no amorphous phase were obtained after a heating time of 20 hr versus 10 h for TPA. However, the TBA template produces larger perfect crystals [19], ~10 micron size, compared to ~ 4 micron size for crystals obtained with TPA (Figure 5.3c). It is evident that the aging time has a greater effect on morphology in the case of TPA than the heating time, whereas both aging and heating times are important when using the TBA template.

Effect of alumatrane content on crystal morphology

We investigated the influence of alumatrane loading on crystal morphology at ratios of Si/Al equal to 75:1, 50:1, 25:1 and 10:1. The other ingredients of the formulation were fixed by correlating to the Si content. Aging times of 60 h at room

temperature and heating time of 10 h at a temperature of 150°C were applied for the TPA template mixture, compared to 84 h and 15 h aging and heating times, respectively, at the corresponding temperatures, for the TBA template system. Figures 5.6 and 5.7 show the change in morphology of crystals using the TBA and TPA systems, respectively, due to the change in alumatrane content.

Several previous works have reported [1,4,10] the difficulty in achieving a perfect crystal MFI at a Si/Al ratio around 10. This was confirmed by our present study. At lower Si/Al ratios, we encountered greater difficulty in MFI synthesis with both TPA and TBA templates. Clearly, introducing higher levels of alumatrane increasingly impedes MFI crystal formation. As seen in Figures 5.6 and 5.7, for both TPA and TBA, the shape of the crystals becomes rounder on increasing the aluminum content. Also evident is the fact that the crystals are more oblong for TBA, which correlates with the expectation that the template molecule affects the growth direction of the crystal, as discussed above. Amorphous aluminosilicate was produced predominantly with the highest alumatrane loading. However, at the Si/Al ratio 10, using the TPA template, some MFI was obtained along with amorphous phase, as seen in Figure 5.7d. With this formulation, lower levels of amorphous phase can be achieved by increasing the heating time or the aging time. This result is consistent with the expectation that TPA is a more efficient template for MFI synthesis. Under comparable conditions, only a Si/Al ratio of 25 enables MFI formation for both TBA and TPA systems.

XRF analysis was applied to confirm the composition of Si and Al in the structure of the MFI, and the result are summarized in Table 5.3. A linear relation is found between the composition loading and the actual Si/Al content. The Si/Al ratio decreases as the alumatrane loading increases though the aluminum content is lower than the actual loading by a similar ratio in every formulation. We further note that the XRF result indicating increasing Al content in the MFI crystal is consistent with the evolution of morphological changes seen by SEM. Finally, Table 5.3 indicates no significant influence of the template structure on the incorporation of Al in the MFI framework.

At the highest loading of Si/Al equal to 10, a sample was prepared with 15 h heating time at 150°C. As indicated in Table 5.3, the resulting material had a high measured aluminum content (Si/Al = 15.3), and a distinctive morphology which appears to consist of many small fused crystallites, as seen in the SEM micrograph in Figure 5.8.

Effect of NaOH concentration

As mentioned previously, either low or high ratio of OH^-/Si gave poor results for the formation of pure silicate MFI. The new question of the influence of the NaOH/Al ratio on MFI morphology was studied by setting the NaOH/Al ratio at 5, 10 and 15, producing the results shown in figure 5.9. The TPA system was chosen due to its superior performance, as discussed above. At Si/Al ratio of 25 with aging time 60 h, it was found that at the highest NaOH/Al ratio, smaller MFI crystals were obtained together with substantial amounts of amorphous phase, whereas larger crystals with a small amount of amorphous were obtained at the lowest NaOH concentration. At the intermediate NaOH concentration, round crystals with little amorphous phase were produced.

From these results, evidently sodium or hydroxide ion concentration influences MFI crystal formation. In earlier work, it was shown that the sodium cation participates in the nucleation step by stabilizing the polysilicate anion, formed as an intermediate [19]. It is also known that, the higher the sodium cation concentration, the more amorphous phase is produced due to steric hindrance between the template and the polysilicate anion (c.f. Figure 5.9c) [11]. We further studied the effect of sodium concentration on crystal morphology, by fixing the formulation at Si/Al/TPA/OH^-/H_2O of 25/1/2.5/10/2850, and varying the Na^+/Al ratio between 10, 15 and 20. The results are shown in figure 5.10. Too high concentration of sodium cation causes retardation of crystal formation, similar to the previous results. As the Na^+ concentration increases, the crystal size increases, and larger amounts of amorphous phase are formed. At the highest Na^+/Al ratio of 20, MFI crystals are rarely formed, as indicated by XRD analysis.

To study the effect of hydroxide concentration, the Na^+/Al ratio was fixed at 10 and the OH^-/Al ratio was varied from 10 to 5 to 2.5. The SEM result is essentially

the same as that shown in figure 5.9a, at the OH^-/Al ratio of 5. This is surprising, considering the fact that the pure silicate MFI with TBA as template gave only amorphous phase under these conditions [19]. On lowering hydroxide concentration to 2.5 OH^-/Al, very few MFI crystals were detected by XRD. It is possible that MFI can form under these conditions because TPA was used in the present study rather than TBA. However, it was observed that with less hydroxide ion the aged sample formed a gel as quickly as a sample without NaOH, i.e. within one hour. In addition, the formation of substantial amounts of amorphous product indicates decreased interaction between precursor and the template.

Though the sodium ion is generally present in zeolite to stabilize the negative charge in the framework structure between Si-O-Al linkages, adding more sodium does not promote more Al ion to incorporate in the structure, as XRF analysis of the crystals shown in figures 5.10a, 5.10b, and 5.10c indicates, for Si/Al ratios of 34.3, 34.3, and 30.5, respectively. Thus, it is clear that excess sodium ions have no effect on the Si/Al ratio. In contrast, by increasing the NaOH/Al ratio from 5 to 10 to 15, XRF analysis of the crystals shown in figures 5.9a, b, and c indicates that the Si/Al ratio decreases from 37.9, to 34.3 and 21.8 respectively. It follows that higher sodium hydroxide concentration can promote more aluminum to incorporate in the zeolite structure.

5.5 Conclusions

Silatrane and alumatrane were synthesized and used as precursors for synthesizing MFI zeolite. Two types of template, TPA and TBA, were studied to compare their effect on the MFI morphology. The TPA shows better performance by decreasing the aging and heating times while showing no significant influence on the Si/Al ratio. Differences in the morphology of MFI were also observed between TPA and TBA, which appear related to differences in steric hindrance of the templates during crystal formation. The Si/Al ratio in MFI zeolite increases linearly relative to the loading composition, however, the aluminum content can be enhanced by formulating with higher sodium hydroxide concentration. Increased alumatrane loading causes more difficulty for MFI crystal formation, however, the tendency for MFI formation is improved by increasing the aging and heating times.

5.6 Acknowledgements

The research work is supported by the Thailand Research Fund (TRF), the Asian Development Bank (ADB) Fund and Ratchadapisakesompoch Fund, Chulalongkorn University.

5.7 References

[1] J. Machado, C.M. Lopez, M.A. Centeno, C.Urbina, Appl. Catal. A 181 (1999) 29.

[2] A. Moini, K.D. Schmitt, and R.F. Polomski, Zeolites 18 (1997) 2.

[3] L.D. Rollmann, J.L. Schlenker, S.L. Lawton, C.L. Kennedy, G.J. Kennedy, D.J. Doren, J. Phys. Chem. B 103 (1999) 7175.

[4] L.D. Rollmann, J.L. Schlenker, C.L. Kennedy, G.J. Kennedy, D.J. Doren, J. Phys. Chem. B 104 (2000) 721.

[5] P.-P.E.A. De Moor, T.P.M. Beelen, and R.A. Van Santen, L.W. Beck, M.E. Davis, J. Phys. Chem. B 104 (2000) 7600.

[6] P.-P.E.A. De Moor, T.P.M. Beelen, R.A. Van Santen, Chem. Mater. 11 (1999) 36.

[7] H.X. Li, M.A. Camblor, M.E. Davis, Microporous Mater. 3 (1994) 117.

[8] R.E. Boyett, A.P. Stevens, M.G. Ford, P.A. Cox, Zeolites 17 (1996) 508.

[9] A. Chatterjee, J. Mole. Catal. A 120 (1997) 155.

[10] A. Arafat, J.C. Jansen, A.R. Ebaid, H. Van Bekkum, Zeolites 13 (1993) 162.

[11] J.H. Koegler, H. Van Bekkum, J.C. Jansen, Zeolites 19 (1997) 262.

[12] J.N. Watson, L.E. Iton, R.I. Keir, J.C. Thomas, T.L. Dowling, J.W. White, J. Phys. Chem. B 101 (1997) 10094.

[13] P.-P.E.A. De Moor, T.P.M. Beelen, R.A. Van Santen, J. Phys. Chem. B 103 (1999) 1639.

[14] R. Ravishankar, C.E.A. Kirschhock, P.-P.K. Gerrits, E.J.P. Feijen, P.J. Grobet, P. Vanoppen, F.C. De Schryver, G. Miehe, H. Fuess, B.J. Schoeman, P.A. Jacobs, J.A. Martens, J. Phys. Chem. B 103 (1999) 4960.

[15] C.E.A. Kirschhock, R. Ravishankar, F. Verspeurt, P.J. Grobet, P.A. Jacobs, J.A. Martens, J. Phys. Chem. B 103 (1999) 4965.

[16] C.E.A. Kirschhock, R. Ravishankar, L. Van Looveren, P.A. Jacobs, J.A. Martens, J. Phys. Chem. B 103 (1999) 4972.

[17] M.J. Verhoef, P.J. Kooyman, J.C. Van Der Waal, M.S. Rigutto, J.A. Peters, H. Van Bekkum, Chem. Mater. 13 (2001) 683.

[18] Z. Wang, Y. Yan, Chem. Mater. 13 (2001) 1101.

[19] P. Phiriyawirut, R. Magaraphan, A. Jamieson, S. Wongkasemjit, Mater. Sci. & Eng., Inpress.

[20] E.V. Burchart, H. Van Koningsveld, B. Van De Graaf, Microporous Mater. 8 (1997) 215.

[21] M. Sathupunya, E. Gulari, S. Wongkasemjit, J. Eur. Cera. Soc. 22 (2002) 2305.

[22] M. Sathupunya, E. Gulari, S. Wongkasemjit, J. Eur. Cera. Soc. 23/8 (2003) 1293.

[23] S. Cabrera, J. El Haskouri, C. Guillem, J. Latorre, A. Beltran-Porter, D. Beltran-Porter, M.D. Marcos, P. Amoros, Solid State Sci. 2 (2000) 405.

[24] Y. Opornsawad, B. Ksapabutr, S. Wongkasemjit, R.M. Laine, Eur. Poly. 37 (2001) 1877.

CAPTIONS OF TABLE AND FIGURES

Table 5.1

m/e	Intensities	Proposed structure
192	100	$N[CH_2CHCH_3OH]_3H^+$ (TIS)
216	6.25	$N[CH_2CHCH_3O]_3H^+Al$ (monomer)
407	11.5	$H^+N[CH_2CHCH_3O]_3AlOH^+CHCH_3CH_2N[CH_2CHCH_3OH]_2$
431	19.25	2 $N[CH_2CHCH_3O]_3H^+Al$ (dimer)
577	1.46	$[HOCHCH_3CH_2N[CH_2CHCH_3O]_2AlOCHCH_3CH_2]_2N^+CH_2$
646	0.38	3 $N[CH_2CHCH_3O]_3H^+Al$ (trimer)

Table 5.2

m/e	Intensities	Proposed structure
174	100	$N[CH_2CH_2O]_3Si^+$
236	11.3	$H_2{}^+OCH_2CH_2OSi[OCH_2CH_2]_3N$
291	1	$N[CH_2CH_2O]_3OSiOCH_2CH_2N^+[CH_2CH_2OH]CH_2$
323	2.6	$H^+[HOCH_2CH_2]_2NCH_2CH_2OSi[OCH_2CH_2]_3N$
409	0.04	$N[CH_2CH_2O]_3H^+SiOCH_2CH_2OSi[OCH_2CH_2]_3N$

Table 5.3

Formulated Composition	Si/Al of MFI with different templates	
Si/Al	TBA	TPA
10	-	15.3*
25	32.0	33.3
50	62.9	64.0
75	91.8	88.0

* Extend heating time to 15 hr

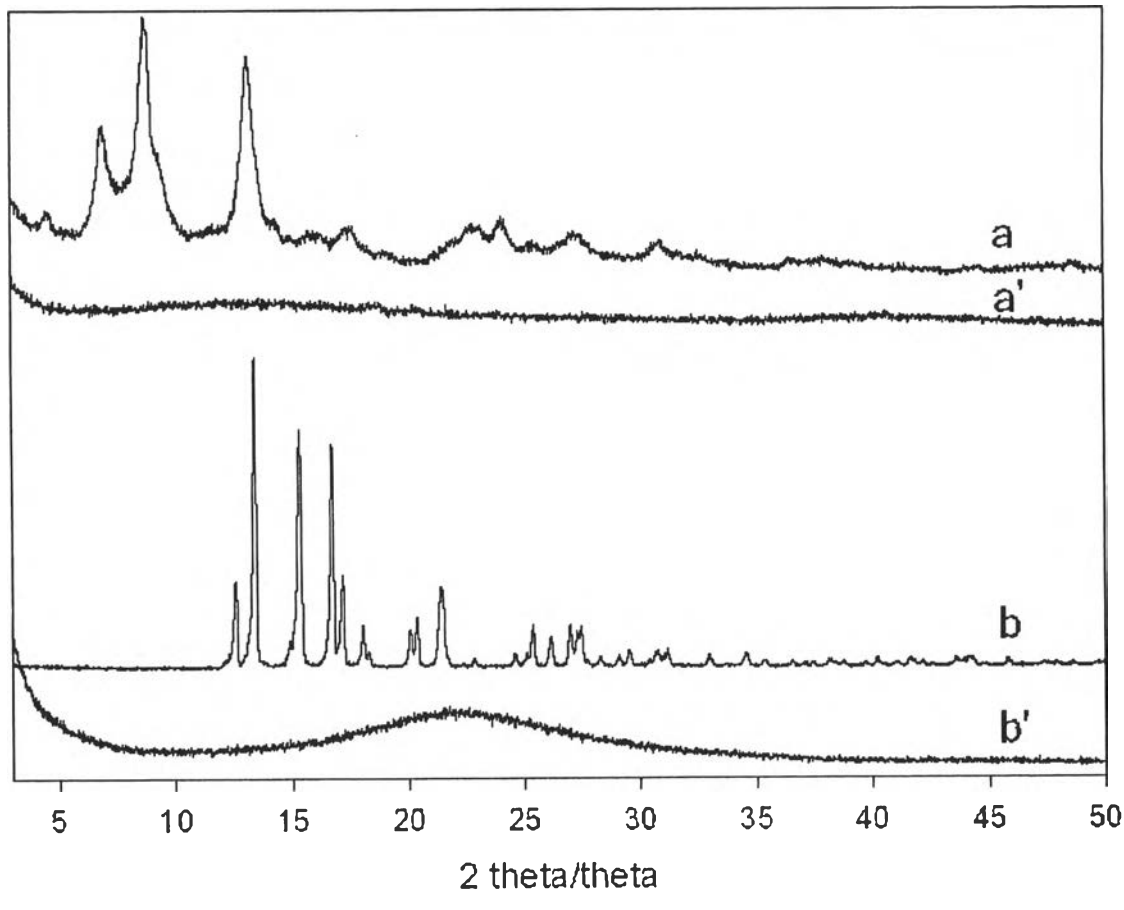

Figure 5.1

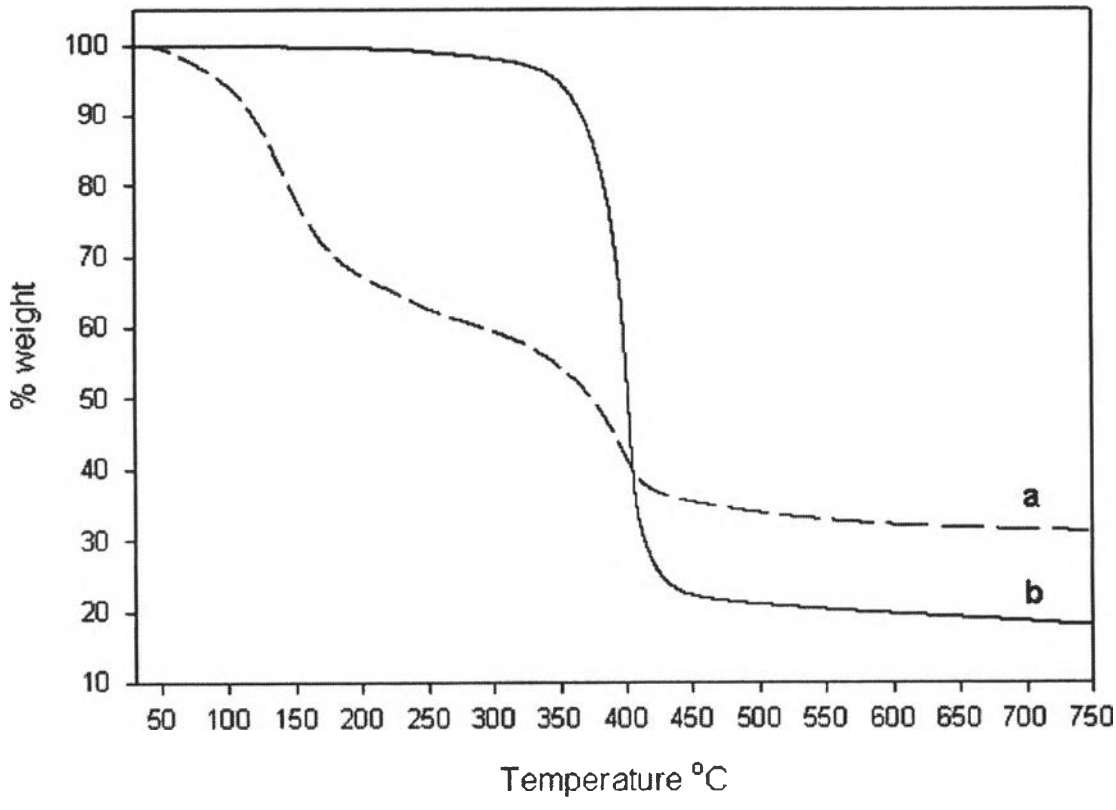
100
90
80
70
60
50
40
30
20
10
% weight
50 100 150 200 250 300 350 400 450 500 550 600 650 700 750
Temperature °C
a
b

Figure 5.2

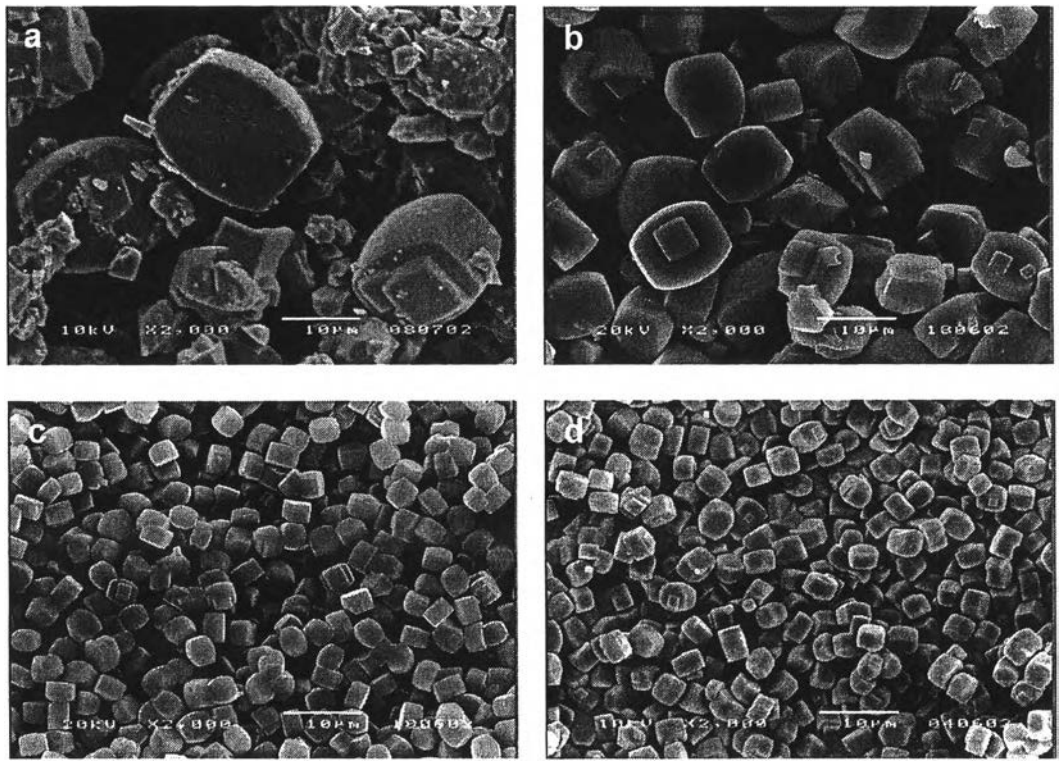

Figure 5.3

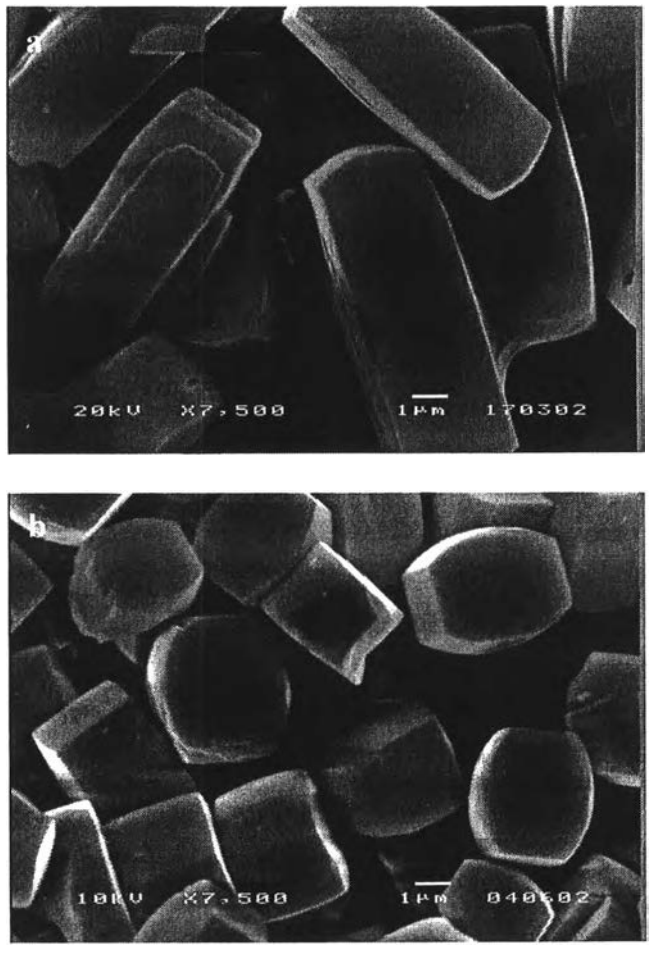

Figure 5.4

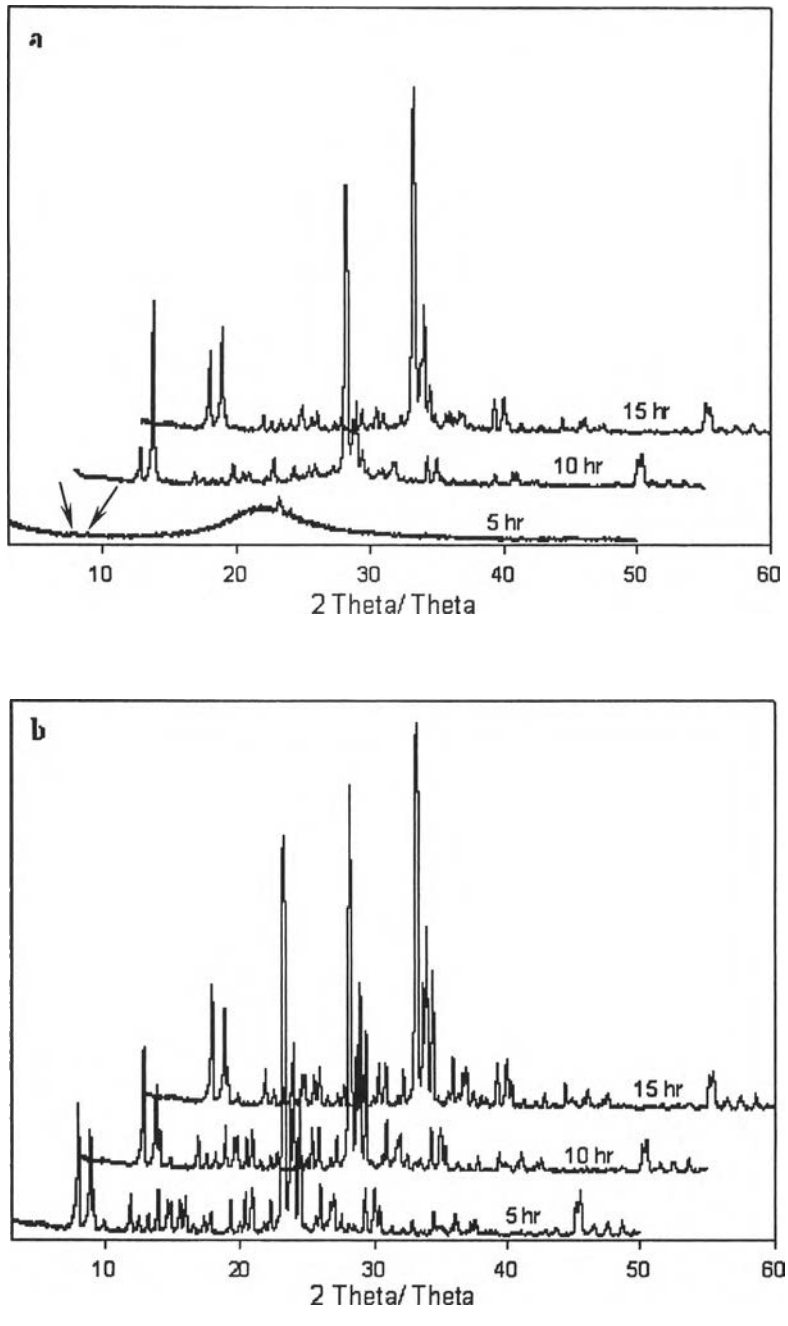
a
15 hr
10 hr
5 hr
10
20
30
40
50
60
2 Theta/ Theta
b
15 hr
10 hr
5 hr
10
20
30
40
50
60
2 Theta/ Theta

Figure 5.5

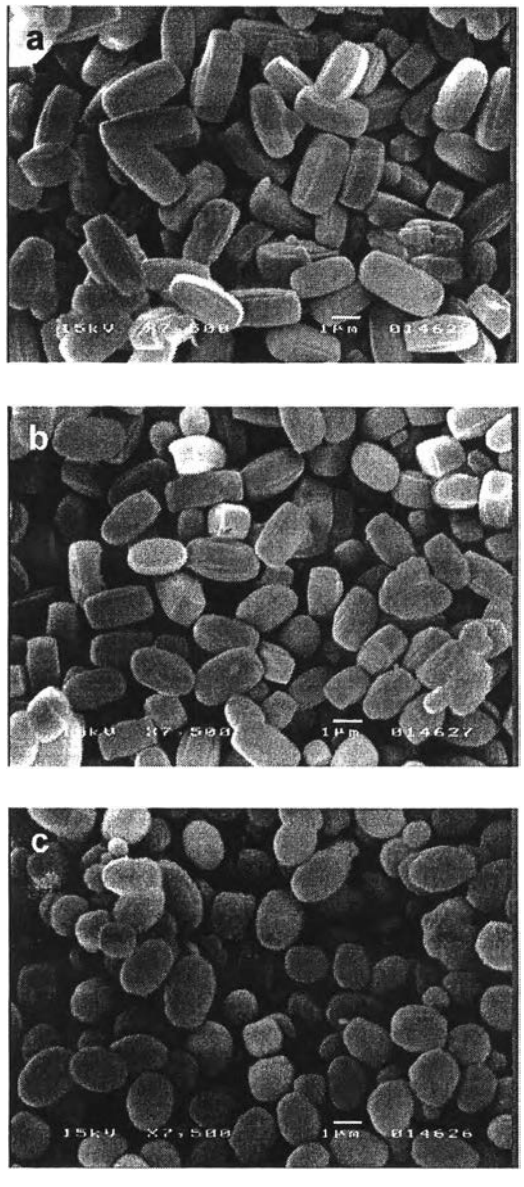

Figure 5.6

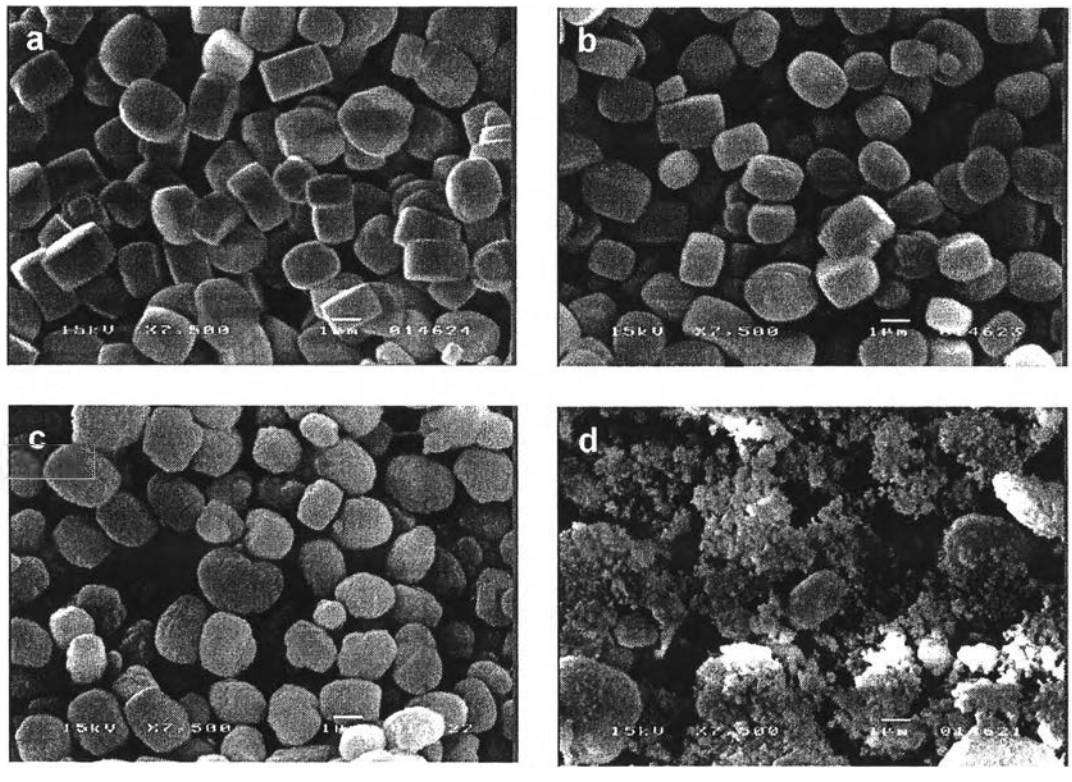
a
15kV X7,500 1μm 014624
b
15kV X7,500 1μm
c
15kV X7,500
d
15kV X7,500

Figure 5.7

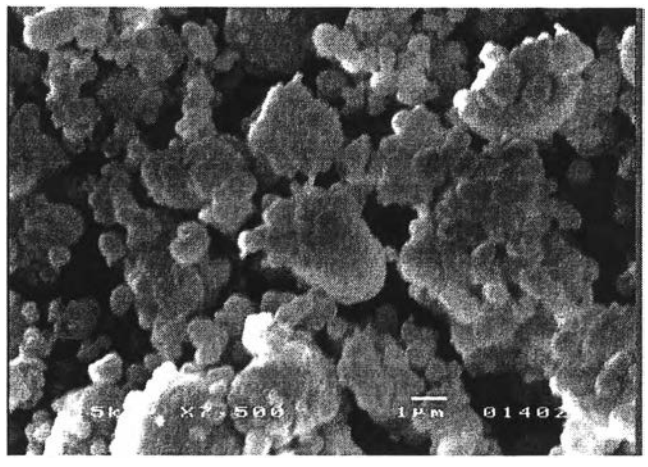

Figure 5.8

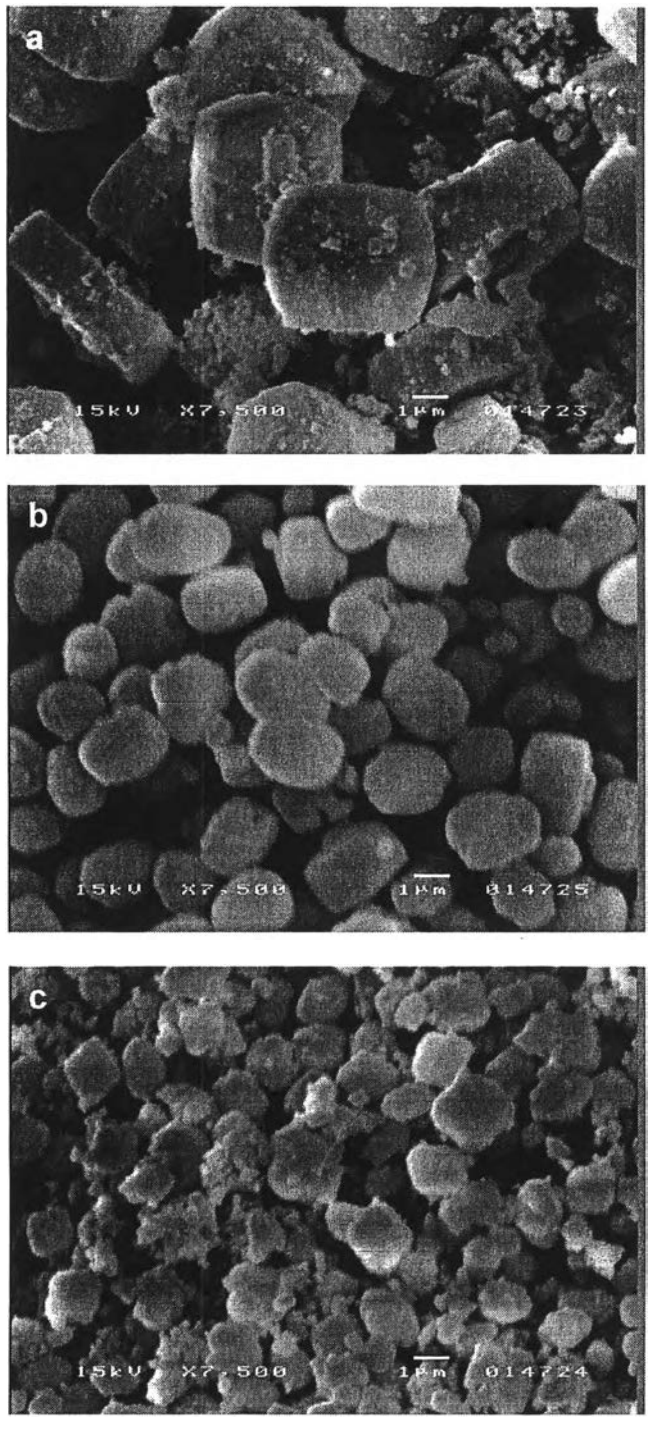
a
15kV X7,500 1µm 014723
b
15kV X7,500 1µm 014725
c
15kV X7,500 1µm 014724

Figure 5.9

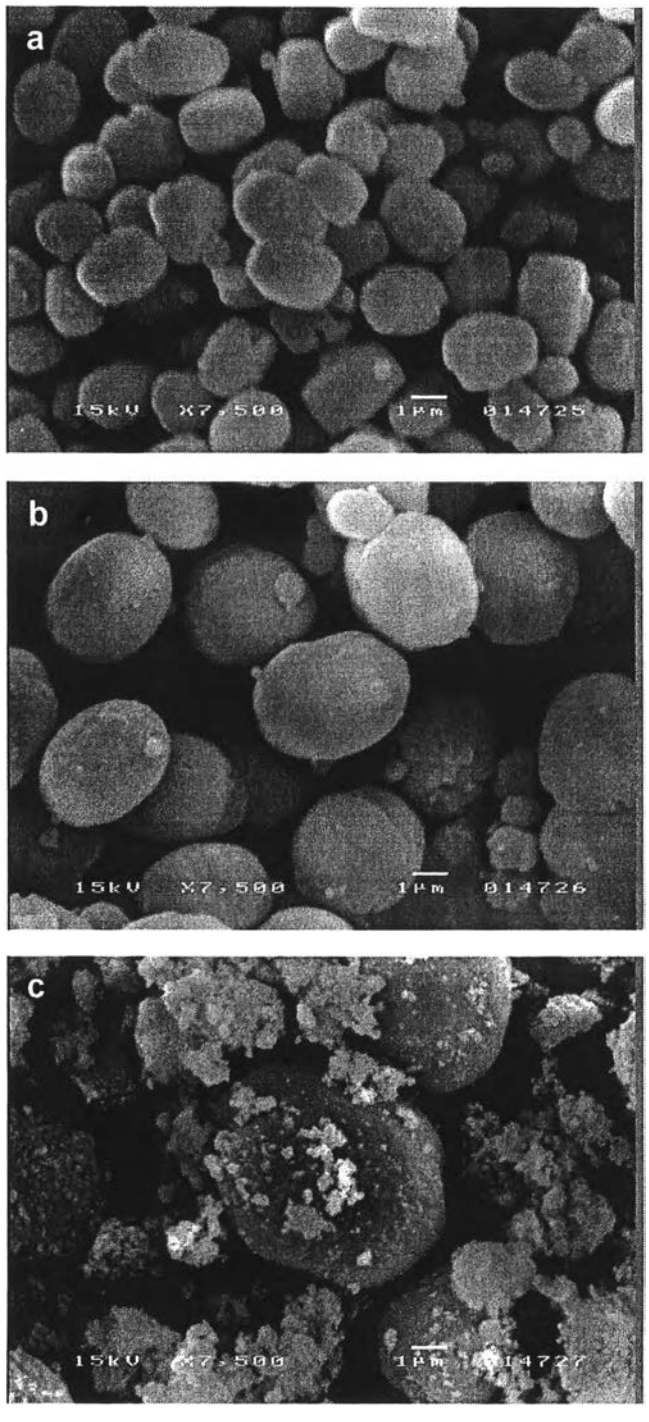
a
15kV X7,500 1µm 014725
b
15kV X7,500 1µm 014726
c
15kV X7,500 1µm

Figure 5.10